1 **Molecular transformations of phenolic SOA during photochemical aging in the**

2 **aqueous phase: competition among oligomerization, functionalization, and**

3 **fragmentation**

4

5 Lu Yu[1], Jeremy Smith[2], Alexander Laskin[3], Katheryn M. George[4], Cort Anastasio[2], Julia

6 Laskin[5], Ann M. Dillner[4], Qi Zhang[1]*

7

8 [1]Department of Environmental Toxicology, University of California, 1 Shields Ave.,

9 Davis, CA 95616, USA

10 [2]Department of Land, Air and Water Resources, University of California, 1 Shields Ave.,

11 Davis, CA 95616, USA

12 [3]Environmental Molecular Sciences Laboratory, Pacific Northwest National Laboratory,

13 Richland, WA 99352, USA

14 [4]Crocker Nuclear Laboratory, University of California, 1 Shields Ave., Davis, CA 95616

15 [5]Physical Sciences Division, Pacific Northwest National Laboratory, Richland, WA

16 99352, USA

17 *Corresponding Author: Qi Zhang, Department of Environmental Toxicology, University

18 of California, 1 Shields Ave., Davis, CA 95616, USA. Tel.: 530-752-5779; fax: 530-752-

19 3394; e-mail: dkwzhang@ucdavis.edu

Abstract

20

21   Organic aerosol is formed and transformed in atmospheric aqueous phases (e.g.,

22   cloud and fog droplets and deliquesced airborne particles containing small amounts of

23   water) through a multitude of chemical reactions. Understanding these reactions is

24   important for a predictive understanding of atmospheric aging of aerosols and their

25   impacts on climate, air quality, and human health. In this study, we investigate the

26   chemical evolution of aqueous secondary organic aerosol (aqSOA) formed during

27   reactions of phenolic compounds with two oxidants – the triplet excited state of an

28   aromatic carbonyl ($^3C^*$) and hydroxyl radical (•OH). Changes in the molecular

29   composition of aqSOA as a function of aging time are characterized using an offline

30   nanospray desorption electrospray ionization mass spectrometer (nano-DESI MS)

31   whereas the real-time evolution of SOA mass, elemental ratios, and average carbon

32   oxidation state (OS_C) are monitored using an online aerosol mass spectrometer (AMS).

33   Our results indicate that oligomerization is an important aqueous reaction pathway for

34   phenols, especially during the initial stage of photooxidation equivalent to ~ 2 hours

35   irradiation under midday, winter solstice sunlight in northern California. At later reaction

36   times functionalization (i.e., adding polar oxygenated functional groups to the molecule)

37   and fragmentation (i.e., breaking of covalent bonds) become more important processes,

38   forming a large variety of functionalized aromatic and open-ring products with higher

39   OS_C values. Fragmentation reactions eventually dominate the photochemical evolution of

40   phenolic aqSOA, forming a large number of highly oxygenated ring-opening molecules

41   with carbon numbers (n_C) below 6. The average n_C of phenolic aqSOA decreases while

42   average OS_C increases over the course of photochemical aging. In addition, the saturation

43 vapor pressures (C^*) of dozens of the most abundant phenolic aqSOA molecules are

44 estimated. A wide range of C^* values is observed, varying from $< 10^{-20}$ μg m^{-3} for

45 functionalized phenolic oligomers to > 10 μg m^{-3} for small open-ring species. The

46 detection of abundant extremely low volatile organic compounds (ELVOC) indicates that

47 aqueous reactions of phenolic compounds are likely an important source of ELVOC in

48 the atmosphere.

49

50 <u>Keywords</u>: particulate matter, hydroxyl radical, triplet excited state, photochemical aging,

51 molecular transformation, AMS, nano-DESI MS

52

53 **1. Introduction**

54   Secondary organic aerosol (SOA), which accounts for a major fraction of fine

55 particle mass in the atmosphere (*Jimenez et al., 2009;Zhang et al., 2007*), is formed and

56 transformed through a multitude of chemical and physical processes (*Ervens et al.,*

57 *2011;Hallquist et al., 2009;Jimenez et al., 2009;Ervens, 2015*). The chemical

58 transformation of SOA can be described by three competing mechanisms −

59 functionalization, fragmentation, and oligomerization (*Kroll and Seinfeld, 2008;Kroll et*

60 *al., 2009*). Functionalization adds polar, oxygenated functional groups to a molecule and

61 generally decreases its volatility; fragmentation breaks covalent bonds in a molecule and

62 tends to increase its volatility; and oligomerization combines two or more molecules

63 through covalent bonds, producing a larger molecule with substantially lower volatility

64 (*Kroll et al., 2009*). While these pathways occur in parallel, oxidative fragmentation

65 usually becomes more important over the course of atmospheric aging, leading to the

66   formation of increasingly more oxidized organic aerosol as well as volatile molecules that

67   are lost from the particles. Analyses of ambient aerosol datasets acquired worldwide with

68   aerosol mass spectrometers (AMS) have indeed shown that less oxidized, semi-volatile

69   oxygenated organic aerosol (SV-OOA) generally evolves into highly oxidized, low-

70   volatility oxygenated organic aerosol (LV-OOA) due to atmospheric aging (*Ng et al.,*

71   *2010;Morgan et al., 2010*).

72   The aging of organic aerosol has been investigated in a number of laboratory and

73   field studies (e.g., *Kroll and Seinfeld, 2008;Jimenez et al., 2009;Renard et al.,*

74   *2015;Morgan et al., 2010*). While most of the studies have so far focused on gas-phase

75   photochemical processes, aqueous reactions are also ubiquitous and can influence aerosol

76   composition and properties significantly (e.g., *Blando and Turpin, 2000;Lim et al.,*

77   *2010;Ervens et al., 2011;Hennigan et al., 2012;Altieri et al., 2012;Zhang and Anastasio,*

78   *2003;Lee et al., 2012;Ge et al., 2012;Ervens, 2015*). Understanding the formation and

79   transformation of SOA through aqueous reactions is therefore important for elucidating

80   the atmospheric evolution of particles and modeling their impacts on climate and human

81   health.

82   In this work we examine the aqueous reactions of phenols, which are a family of

83   lignin-derived compounds emitted in large quantities from biomass burning (*Hawthorne*

84   *et al., 1989;Schauer et al., 2001*). Oxidation of aromatic hydrocarbons in anthropogenic

85   emissions can also lead to the formation of phenols (*Graber and Rudich, 2006*). Studies

86   have shown that volatile phenols and benzene-diols are rapidly oxidized by hydroxyl

87   radical ($\cdot$OH), nitrate radical (NO$_3\cdot$), and excited triplet states (^{3}C*) of aromatic carbonyls

88   in the aqueous phase (*Herrmann, 2003;Anastasio et al., 1997*), forming aqSOA (i.e., low

89   volatility species formed via aqueous reactions of volatile precursors) with high mass

90   yields (*Smith et al., 2014;Smith et al., 2015;Sun et al., 2010*). The lifetimes of phenols

91   with respect to $^3C^*$ and •OH reactions in atmospheric fog and cloud water are on the

92   order of minutes to hours during daytime (*Smith et al., 2014*), which is of the same order

93   as the gas phase oxidation of phenols (i.e., hours) (*Feigenbrugel et al., 2004*).

94   Furthermore, recent studies in our group have shown that the aqSOA of phenols are

95   highly oxidized, with average atomic oxygen-to-carbon (O/C) ratios of ~ 1 and are

96   comprised of a large number of water-soluble molecules with polar functional groups

97   including carbonyl, carboxyl, and hydroxyl groups (*Sun et al., 2010;Yu et al.,*

98   *2014;George et al., 2015*). This is an indication that phenolic aqSOA can influence the

99   hygroscopicity of ambient particles and thus their cloud formation potential. In addition,

100   phenolic aqSOA show enhanced light absorption in the UV-vis region compared to their

101   precursors (*Chang and Thompson, 2010;Yu et al., 2014*), which suggests that they are

102   likely an important component of brown carbon in the atmosphere (*Laskin et al.,*

103   *2015;Andreae and Gelencsér, 2006*), especially in regions influenced by biomass burning

104   emissions. Despite this, little is known about how the chemical composition and physical

105   properties of phenolic aqSOA evolve as a function of photochemical age in the

106   atmosphere.

107   We investigate the chemical evolution of aqSOA formed from the three basic

108   structures of phenols (phenol, guaiacol, and syringol) during reactions with two major

109   aqueous-phase oxidants – $^3C^*$ and •OH. Note that we use the generic term "phenol" in

110   this paper to refer to all phenolic compounds and the abbreviations PhOH, GUA, and

111   SYR to specifically refer to phenol (C_6H_6O), guaiacol ($C_7H_8O_2$; 2-methoxyphenol), and

112 syringol ($C_8H_{10}O_3$; 2,6-dimethoxyphenol), respectively (see their structures in Table 1).

113 The photochemical evolution of aqSOA mass and bulk composition is monitored using

114 an Aerodyne high-resolution (~ 5000 m/Δm) time-of-flight aerosol mass spectrometer

115 (HR-ToF-AMS, hereinafter referred to as AMS), while the molecular transformations of

116 phenolic aqSOA are characterized using high-resolution (~ 100,000 m/Δm at *m/z* = 400)

117 nanospray desorption electrospray ionization mass spectrometry (nano-DESI MS) (*Roach*

118 *et al., 2010a, b*). We examine the relationships between the average carbon oxidation

119 state (OS_C; (*Kroll et al., 2011*)) and number of carbon atoms (n_C) for aqSOA molecules

120 observed during three different stages of aging to gain insights into the photochemical

121 evolutions of phenolic aqSOA. In addition, the volatilities of the 50 most abundant

122 molecules are estimated for each sample and a two-dimensional volatility basis set (2D-

123 VBS) is used to describe the chemical evolution of phenolic aqSOA based on its

124 volatility and O/C ratio (*Donahue et al., 2012;Jimenez et al., 2009*).

125 **2. Experimental Methods**

126 *2.1 Photochemical experiments and chemical analysis*

127   Aqueous oxidations were carried out using air-saturated solutions in stirred 110

128 mL Pyrex tubes under simulated sunlight illumination inside the RPR-200 Photoreactor

129 System discussed in George et al. (*2015*). The initial solution contained 100 μM of a

130 single phenol (i.e., PhOH, GUA, or SYR) and was adjusted to pH 5 using sulfuric acid.

131 The initial concentration of phenol we chose is atmospheric relevant since the

132 concentration of phenols and substituted phenols in cloud and fog waters were found to

133 be in the range of 0.1-30 μM (*Anastasio et al., 1997;Sagebiel and Seiber, 1993*) and in

134 areas impacted by wood burning (e.g., in Northern California during wintertime),

135 concentrations exceeding 100 µM was predicted in fog waters (*Anastasio et al., 1997*).

136 The pH of 5 is within the range of pH values observed in fog and cloud waters (*Collett et*

137 *al., 1999*). Aqueous SOA was formed and evolved using two separate oxidants: 1) adding

138 100 µM hydrogen peroxide (HOOH) to the initial solution as a source of •OH, and 2)

139 adding 5 µM 3,4-dimethoxybenzaldehyde (3,4-DMB) as a source of $^3C^*$. 3,4-DMB was

140 chosen to represent non-phenolic aromatic carbonyls, which are emitted in large

141 quantities from wood burning (*Schauer et al., 2001*), exist nearly exclusively in

142 condensed phases in the atmosphere, and rapidly form $^3C^*$ that efficiently oxidizes

143 phenols (*Anastasio et al., 1997*). The concentrations of phenols and 3,4-DMB are

144 measured using a high-performance liquid chromatograph (HPLC) with a UV-visible

145 detector. Details of the instrumentation and methodology are reported in Smith et al.

146 (*2014*). In addition, 10.0 mg L^{-1} ammonium sulfate was added to each solution as an

147 internal standard to relate aerosol concentration (µg m^{-3}) measured by AMS to liquid

148 concentration (mg L^{-1}).

149 In order to compare the photochemical kinetics in the RPR-200 Photoreactor

150 System with that in the ambient, we calculated the steady-state concentrations of •OH

151 and the rate constant for the formation of $^3C^*$ in the RPR-200 Photoreactor System.

152 Detailed information is given in George et al. (*2015*). For $^3C^*$ exposure, the rate of light

153 absorption is ~7 times faster in the RPR-200 Photoreactor System than that in the midday

154 winter solstice sunlight in Davis. The •OH steady-state concentration in the RPR-200

155 Photoreactor System under the reaction condition is ~6.5 times higher than the average

156 fog water value, which is normalized to Davis winter solstice sunlight. Thus, the lifetime

7

157 of phenolic precursors is ~6.5 times longer in the ambient fog water than that in RPR-200

158 Photoreactor System.

159   Through the course of each experiment, a Shimadzu LC-10AD high-performance

160 liquid chromatography (HPLC) pump was used to draw solution at a constant flow rate

161 (1.0 mL min^{-1}) alternatively from three identical illuminated tubes (total volume = 345

162 mL) and one dark control tube covered with aluminum foil. The solution was delivered to

163 a Collison atomizer, where pressurized argon was used to atomize the solution. The

164 resulting aerosol was fully dried using a diffusion dryer and then divided into two flows.

165 One aerosol flow was sampled and analyzed in real-time by AMS at 1 min time

166 resolution and the other passed through a Teflon filter to collect particles for offline

167 analyses using nano-DESI MS. Three filters were collected at different time intervals

168 over the course of each experiment; the sampling interval for each filter is given in Table

169 1. For SYR and GUA experiments, the illuminated solution was continuously aerosolized

170 and sampled until it was exhausted after ~ 6 hours. Since PhOH is much less reactive

171 than SYR and GUA, with a 4 – 30 times longer half-life ($t_{1/2}$) in aqueous phase (*Smith et*

172 *al., 2014;Yu et al., 2014*), we conducted the PhOH experiments for a total of 20 – 24

173 hours by sampling the illuminated solution at 50% duty-cycle (i.e., on and off every hour)

174 during the first 9 – 12 hours and the last 2 hours of the experiment. Sampling was halted

175 for ~ 10 hours while the solution was continuously illuminated. Details of AMS and

176 nano-DESI MS measurements are given in Yu et al. (*2014*) and included in the

177 Supporting Information. During each experiment, aliquots of the illuminated solution

178 were also collected at defined time intervals and analyzed offline using an HPLC

179 equipped with a UV-vis detector to monitor phenol concentrations.

8

180   *2.2 Determination of phenol reaction rates and aqSOA formation rates*

181   The initial rates of aqSOA formation and phenolic precursor decay were

182   determined using an appropriate fit performed with Igor Pro 6.36 (Wavemetrics, Portland,

183   OR, USA). The measured apparent first-order rate constant for phenol loss (k_d) was

184   determined using an exponential decay fit to Eqn. 1:

185     $$[ArOH]_t / [ArOH]_0 = \exp(-k_d\, t) \tag{1}$$

186   where $[ArOH]_t$ and $[ArOH]_0$ are the measured concentrations of phenol at times t and 0,

187   respectively. The initial destruction rate (i.e., at $t = 0$) of phenol was therefore calculated

188   as: $R_d = k_d \times [ArOH]_0$.

189   The apparent formation rate constant of phenolic aqSOA (k_f) was determined by

190   fitting a three-parameter exponential rise to a maximum equation to the experimental data

191   (*Zhang and Anastasio, 2003*):

192     $$[aqSOA] = a - b\, \exp(-k_f\, t) \tag{2}$$

193   where [aqSOA] is the concentration of aqSOA at time t, and a, b, and k_f are fitted

194   parameters. The apparent initial formation rate of aqSOA was calculated as: $R_f = b \times k_f$.

195   *2.3 Determination of aqSOA elemental ratios, OS_C and n_C*

196   The average atomic ratios of oxygen-to-carbon (O/C) and hydrogen-to-carbon

197   (H/C) in bulk aqSOA were determined using AMS mass spectra (*Aiken et al., 2008*).

198   Since we used argon as a carrier gas and removed physically-bonded water molecules

199   from the particles, we were able to determine the abundances of CO^+ and H_2O-related

200   ions (i.e., H_2O^+, HO^+, and O^+) in the spectra of phenolic aqSOA directly (*Yu et al.,*

201   *2014;Sun et al., 2009*). Thus, the O/C and H/C of aqSOA were determined without

202   assuming relationships among CO^+, H_2O^+ and CO_2^+. Since the phenolic aqSOA in this

203   study are made up of only C, H, and O. In addition, the amount of peroxide groups

9

204 appears to be negligible based on nano-DESI MS analysis. Thus, the average OS_C is

205 equal to $2 \times O/C - H/C$ (*Kroll et al., 2011*). According to Aiken et al. (*2008*), the average

206 errors in the O/C and H/C values measured by the AMS are 31% and 10%, respectively.

207 The propagated error in OS_C is estimated at 33%.

208   The molecular formulas of hundreds of individual aqSOA species were derived

209 from nano-DESI MS acquired in the negative ion mode. The average O/C, H/C, and

210 number of carbon atoms (n_C) in a given aqSOA sample were subsequently calculated by

211 averaging across the individual values of each species weighted by the corresponding ion

212 abundances in nano-DESI MS (*Bateman et al., 2012*). Comparisons of the average O/C,

213 H/C, and OS_C of aqSOA determined by AMS and nano-DESI MS are discussed in

214 Appendix A.

215 ***2.4 Estimation of volatilities of aqSOA molecules***

216   Based on the negative ion mode nano-DESI MS, we identified the 50 most

217 abundant phenolic aqSOA molecules in each sample and estimated their volatilities. The

218 molecular structure of each compound was proposed based on its molecular formula,

219 double bond equivalent ($DBE = C - H/2 + 1$), and chemical reasonability of the structure.

220 The vapor pressures of the compounds at 298.15 K were subsequently estimated based on

221 the Nannoolal vapor pressure and extrapolation method (*Nannoolal et al.,*

222 *2008;Nannoolal et al., 2004*) using the predictor available at

223 http://www.aim.env.uea.ac.uk/aim/ddbst/pcalc_main.php).

10

3. Results and discussion

3.1 Photochemical evolution of aqSOA mass and elemental compositions

Figure 1 provides an overview of the dynamics of phenol decay, aqSOA formation, and the evolution of aqSOA bulk composition (i.e., O/C, H/C, and OS_C) during each experiment. The reactions appear to follow first-order kinetics reasonably well (Figs. 1a-c) and the fitted rate constants and initial reaction rates are given in Table 2. Among all reactions, SYR + $^3C^*$ is the fastest (k_d = 2.0 hr^{-1} and R_d = 30 mg-SYR L^{-1} hr^{-1}, Table 2) and produces aqSOA at the highest rate (k_f = 1.1 hr^{-1} and R_f = 16 mg-aqSOA L^{-1} hr^{-1}). PhOH is much less reactive than SYR and forms aqSOA at initial rates more than 10 times slower. However, the slow reactions of PhOH allow the precursor to last longer and form aqSOA with higher overall yields (Fig. 1c). For instance, the aqSOA yields from SYR reactions peak at 80% - 100% after 3 - 4 hours (Fig. 1a) while PhOH continues to produce aqSOA beyond 20 hours of illumination with maximum yields reaching 140% (Fig. 1c). In a similar vein, under our conditions $^3C^*$ generally forms aqSOA more quickly than •OH for phenols (Table 2), although the increase in aqSOA mass tends to persist longer in •OH-mediated reactions.

As shown in Fig. 1d-l, the chemical composition of aqSOA evolves continuously throughout the course of photochemical aging. Note that H/C, O/C, and OS_C are not reported for the beginning 10-15 min of the reactions because the aqSOA masses are low here, making the elemental ratios highly uncertain. Highly oxidized aqSOA species are formed immediately after the reactions start and the average O/C of aqSOA are 0.26 – 0.49 higher than the corresponding precursors after only 10-15 min of reactions (Fig. 1d-f). The quick formation of aqSOA is probably due to fast oligomerization coupled with addition of oxygenated functional groups. Indeed, previous studies have shown that

11

248   phenolic aqSOA present after illumination for one half-life, which vary between ~ 20 min

249   for SYR +^{3}C* and ~ 6 hr for PhOH reactions (Fig. 1a-c), are mainly composed of dimer,

250   higher oligomers and aromatic derivatives with a variety of oxygenated functional groups

251   (*Sun et al., 2010;Yu et al., 2014;George et al., 2015*). The H/C values of aqSOA are also

252   higher than those of the precursors (Fig. 1g-i), suggesting hydrogen incorporation

253   mechanisms which include electrophilic addition of the •OH radical to the double bonds

254   and electrophilic aromatic substitution reactions to attach more hydrogen-rich functional

255   groups such as –OCH$_3$ or –C(=O)CH$_3$ to the benzene ring. This hypothesis is consistent

256   with the results that the H/C of aqSOA are generally higher in •OH-mediated reactions

257   compared to ^{3}C* reactions for the same precursor (Fig. 1g-i), since •OH-mediated

258   reactions favor the open-ring process (*Yu et al., 2014*).

259   The O/C and OS$_C$ of aqSOA increase throughout the reactions (Figs. 1d-f & 1j-l),

260   indicating the formation of increasingly more oxidized products over time. It is

261   interesting to note that for the reactions of SYR with ^{3}C* and •OH, the precursor is

262   exhausted after 2.5 – 4 hours of illumination (Fig. 1a) and a slow decay of aqSOA occurs

263   shortly afterwards. By performing an exponential decay fit to the aqSOA curve between

264   3.1 – 5.9 hr, the lifetime of SYR aqSOA initiated with ^{3}C* is estimated to be ~ 5.3 hr.

265   However a caveat is that the actual lifetime of aqSOA is likely shorter since 3,4-DMB

266   was photochemically transformed, although at a much slower rate than SYR, during our

267   experiment. For example, measurements of 3,4-DMB concentration indicate that ~ 70%

268   of the original amount reacted after ~ 6 hours of illumination (Fig. S1) and the products

269   could include low volatility species. GUA and PhOH, on the other hand, are not fully

270   depleted throughout the experiments, and no plateau or decrease of aqSOA mass is

271   observed (Fig. 1b & 1c). These results suggest that the overall rate of fragmentation

272   reactions, which can convert some aqSOA species into semi-volatile and volatile

273   molecules, is dependent on aqSOA concentration and that the production of phenolic

274   aqSOA due to functionalization and oligomerization outweighs the loss of aqSOA due to

275   fragmentation before the precursors are consumed.

276   *3.2 Molecular transformation during photochemical aging*

277   In order to gain further insights into the reaction mechanisms of phenolic aqSOA

278   formation and aging, we used nano-DESI MS to investigate the molecular compositions

279   of the aqSOA samples for each of the six phenol/oxidant combinations, with 3 samples

280   collected over defined time intervals during each experiment. Figure 2 shows the

281   negative ion mode nano-DESI mass spectra of these samples from which we calculate the

282   signal-weighted average molecular formula for each sample. Table 1 summarizes the

283   chemical characteristics of phenolic aqSOA during the different reaction stages. In

284   addition, the molecular information of the 10 most abundant compounds in each aqSOA

285   sample identified in the negative ion mode nano-DESI mass spectra are shown in Tables

286   3 and S1-S5.

287   Phenolic dimers and higher oligomers are detected in aqSOA from all stages of

288   reactions, but these molecules become relatively less abundant at longer reaction times.

289   This trend is seen more clearly in Fig. S2, where the signal-weighted distributions of

290   SYR, GUA, and PhOH aqSOA formed during different stages of photoreactions are

291   shown based on the degree of oligomerization. There is a general trend that amounts of

292   dimer, higher oligomers and related derivatives decrease with reaction time, while

293   oxygenated monomeric derivatives and open-ring species are significantly enhanced (Fig.

294   2). For example, as shown in Fig. 2a and 2b, SYR dimer ($C_{16}H_{18}O_6$; MW = 306.1) is the

13

295   most abundant species during the first 2 hours of reaction, but is absent in stages P2 (2-4

296   hr) and P3 (4-6 hr). In the meantime, the relative abundances of functionalized dimer

297   molecules (e.g., $C_{15}H_{16}O_9$; MW = 340.1) and an open-ring species of SYR dimer (e.g.,

298    $C_{15}H_{18}O_7$; MW = 310.1) show significant enhancements during P2 and P3, indicating that

299   aqueous reactions both form and transform SYR oligomers. Similar behavior for the

300   oligomeric products are also observed in the reactions of GUA and PhOH (Fig. 2b-f;

301   Table S1-S5), emphasizing the important role of oligomerization in forming phenolic

302   aqSOA. During later stages of the reactions, the relative abundances of smaller, more

303   oxidized aqSOA molecules, especially those with molecular weights (MW) less than 200

304   Da and O/C > 0.8, increase substantially (Fig. 2), indicating that fragmentation reactions

305   become more dominant over the course of photochemical aging. As shown in Table 1, the

306   average carbon number (n_C) of aqSOA from all experiments decreases during aging. The

307   average molecular weight (MW) of aqSOA shows a similar decreasing trend for SYR,

308   but often shows a peak at the intermediate illumination time for GUA and PhOH. For

309   example, during the reaction of SYR + $^3C^*$ (Fig. 2a), the average molecular formula of

310   the aqSOA formed between 0-2 hours is $C_{14.1}H_{14.2}O_{8.2}$ (MW = 314.7). Upon further

311   illumination, from 2 to 4 hours, the average n_C and MW decrease to 11.4 and 273.5 Da,

312   respectively, corresponding to an average molecular formula of $C_{11.4}H_{11.8}O_{7.8}$. For the last

313   reaction stage of illumination (4-6 hrs), the average n_C and MW continue to decrease and

314   the average molecular formula becomes $C_{10.8}H_{11.4}O_{7.5}$ (average MW = 261.1; Table 1 and

315   Fig. 2).

316   The molecular information of the 10 most abundant compounds in SYR + $^3C^*$

317   aqSOA identified in the positive ion mode nano-DESI mass spectra is shown in Table S6.

14

318   Note that the positive ion mode nano-DESI MS results give similar molecular formulas

319   for the dominant dimer and dimeric derivatives as detected by the negative ion mode

320   measurements. However, a number of open-ring species that have high abundance in the

321   negative nano-DESI mass spectra are not detected among the top 10 most abundant

322   products in the positive ion mode nano-DESI spectra. This is likely due to the fact that

323   open-ring species, such as organic acids, are more likely to deprotonate than protonate,

324   and therefore they are more likely to be detected in the negative ion mode nano-DESI MS

325   analysis.

326   Previous study suggests that oligomerization could potentially occur during the

327   electrospray ionization process (*Yasmeen et al., 2010*). In this study, we analyzed the

328   dark control solution samples using direct infusion ESI-MS analysis. Dimer and higher

329   oligomers are not identified in the ESI mass spectra of dark control samples. In addition,

330   tracer ions of dimer and high oligomers are also identified in the AMS spectra of

331   phenolic aqSOA generated during reaction at half-life (*Yu et al., 2014*). Thus, it is certain

332   that the phenolic oligomers observed in this study are generated through aqueous

333   photochemistry rather than being an artifact of the ESI process.

334   *3.2.1. Photochemical aging of phenolic aqSOA in the $OS_C – n_C$ framework*

335   The average carbon oxidation state, OS_C, has been proposed as a metric for

336   describing the chemistry of atmospheric organic aerosol and its relationship to n_C reveals

337   useful insights into the chemical aging of OA (*Kroll et al., 2011*). We therefore examined

338   the molecular compositions of aqSOA molecules in the OS_C vs. n_C space during different

339   stages of aging for each sample analyzed by nano-DESI MS. Figure 3 shows an example

340   of this for the aqSOA of SYR + $^3C^*$; the OS_C vs. n_C plots for the other 5 experiments are

341   shown in Figs. S3-S7. These figures show that the aqSOA of phenols are composed of

15

342   molecules with a wide range of n_C and OS_C, partially overlapping with regions

343   corresponding to ambient LV-OOA and SV-OOA reported as Kroll et al. (*2011*). There is

344   very little overlap between aqSOA and BBOA (despite the fact that phenols are a major

345   constituent in biomass burning emissions (*Schauer et al., 2001*)) and no overlap between

346   aqSOA and HOA in this space (Figs. 3 and S3-S7), consistent with the fact that primary

347   and secondary organic aerosols are very different chemically, especially in terms of

348   oxidation degree. The OS_C – n_C diagrams also show that with increasing reaction time,

349   the abundance of highly oxidized small molecules with $n_C < 6$ is significantly enhanced,

350   while the abundance of less oxidized, high molecular weight species with $n_C > 18$ is

351   significantly reduced.

352   Since phenolic aqSOA include thousands of continuously evolving product

353   molecules, we further simplify the evolution pattern by mapping the average OS_C and n_C

354   of phenolic aqSOA at different stages of photoreactions onto the OS_C - n_C space (Fig. 4).

355   It is a general trend that photochemical aging converts phenolic aqSOA into smaller and

356   more oxidized species. In addition, the average OS_C values of phenolic aqSOA all fall

357   within the range observed for ambient SOA and increase with aging time, generally

358   moving in the direction from SV-OOA toward LV-OOA. Note that we observe good

359   agreement between nano-DESI MS and AMS average OS_C, as discussed in Appendix A.

360   *3.2.2. Photochemical aging of phenolic aqSOA in the O/C – H/C framework*

361   The molecular transformation of phenolic aqSOA can also be examined in the

362   O/C vs. H/C space using Van Krevelen diagrams (Fig. 5). As illustrated by the SYR +

363   $^3C^*$ reaction, the initial aqSOA (0 – 2 hours of photoreaction) is dominated by large

364   molecules ($n_C > 14$) located in the lower part of the diagram (lower O/C; Fig. 5a), while

365   aqSOA in the last time interval (4 – 6 hours) is dominated by highly oxidized open-ring

16

366   species ($n_C < 6$), with most signal located in the upper part of the diagram (higher O/C).

367   Based on n_C and DBE, these highly oxidized small molecules are likely carboxylic acids

368   formed from the oxidation and fragmentation of larger molecules (Table 3). These results

369   indicate that longer aging leads to more oxidation, functionalization and fragmentation.

370   Fragmentation eventually gains importance over functionalization, forming a large

371   number of highly oxidized open-ring species ($n_C < 6$) by the final time. This is also

372   consistent with AMS results, which show quick formation of aqSOA due to

373   oligomerization and functionalization, followed by fragmentation, and a general decrease

374   in aqSOA mass, at later times (see Sect. 3.1). These results are consistent with previous

375   findings that the higher MW oligomeric SOA compounds are subjected to

376   photodegradation via photolysis (*Romonosky et al., 2015;Lee et al., 2014*).

377   *3.3 Volatility distribution and transformation with photochemical aging*

378   Since the chemical composition of aqSOA evolves with photochemical aging, we

379   also investigated how these transformations affect the volatility of phenolic aqSOA.

380   Saturation concentrations (C^*, µg m^{-3}) were estimated for the 50 most abundant aqSOA

381   species in each phenol/oxidant combination, as shown in Fig. 5 in an O/C vs. $\log_{10}$ (C^*,

382   µg m^{-3}) volatility basis set space (*Pankow and Barsanti, 2009*). The C^* of these molecules

383   vary by $\sim 10^{23}$, ranging from $< 10^{-22}$ µg m^{-3} (e.g., functionalized phenolic oligomers) to $>$

384   10 µg m^{-3} (e.g., highly oxygenated open-ring species with $n_C < 6$). The volatility

385   distribution clearly changes during photochemical aging. For example, SYR aqSOA

386   formed at the initial stage is dominated by the dimer and oxygenated derivatives with C^*

387   values corresponding to the low-volatility (LVOC; $C^* = 3.2 \times 10^{-4} - 0.32$ µg m^{-3};

388   (*Donahue et al., 2012*)) and extremely low-volatility organic compounds (ELVOC; $C^* <$

389   3.2×10^{-4} µg m^{-3}; (*Donahue et al., 2012*)) regions. After ~ 4 hours of illumination, the

390   number and abundance of intermediate-volatility (IVOC; $C^* = 320 - 3.2 \times 10^6$ µg m^{-3};

391   (*Donahue et al., 2012*)) and semi-volatile (SVOC; $C^* = 0.32 - 320$ µg m^{-3}; (*Donahue et*

392   *al., 2012*)) highly oxygenated open-ring species ($n_C < 6$) are significantly enhanced.

393   However, some of the high n_C compounds, such as dimeric derivative $C_{15}H_{16}O_9$, which is

394   classified as an ELVOC according to C^*, still remain in large abundance at the later stage.

395   This is consistent with AMS results, which show that although photochemical aging leads

396   to a slight decrease of SYR aqSOA mass after the precursor is consumed, significant

397   amount of aqSOA mass still remain after illumination equivalent to several days of

398   tropospheric aging (more details are discussed in Sect. 3.1). These results suggest that the

399   photochemical aging increases the volatility of aqSOA by forming a large number of

400   intermediate-volatile and semi-volatile open-ring species ($n_C < 6$), while a number

401   compounds with extremely low volatility are relatively recalcitrant.

402   ### 3.4 Conclusions and atmospheric implications

403   In this study, we investigated the molecular transformations of phenolic aqueous

404   SOA during oxidative aging. Overall, aqueous reactions of phenols form highly oxidized

405   aqSOA at fast rates and aqSOA becomes increasingly oxidized during continued

406   oxidative processing. In order to compare our results with atmospheric observations, in

407   Fig. 6a we map the aqueous aging of phenolic aqSOA on the f_{44} (ratio of ion signal at *m/z*

408   = 44 to total organic signal in the mass spectrum) vs. f_{43} (defined similarly) space. Ng et

409   al. (*2010*) used the f_{44} vs. f_{43} space ("triangle plot") to present the OA factors from PMF

410   analysis of 43 Northern Hemisphere AMS datasets of organic aerosol. In the triangle plot,

411   the less aged SV-OOA generally occupies the broader base of the triangle (likely due to

412   the variable composition of fresher SOA formed from site-specific precursors and

413   sources) and the highly oxidized, more atmospherically aged LV-OOA occupies the

18

414　narrowing top region of the triangle. Our results show that aqueous reactions of phenols

415　produce highly oxidized species with f_{44} values close to ambient LV-OOA but lower f_{43}

416　(Fig. 6a). The evolution pathways of phenolic aqSOA formed under the different reaction

417　conditions all move upward in this space, and have a tendency to converge towards the

418　peak of the triangle. These results are consistent with previous findings that ambient

419　oxidation eventually leads to the formation of OOA with similar chemical composition

420　regardless of the source (*Ng et al., 2010*). Figure 6b shows the Van Krevelen diagram of

421　the average elemental ratios of phenolic aqSOA measured by AMS for the $^3C^*$- and •OH-

422　mediated reactions. The O/C and H/C ratios of phenolic aqSOA appear to evolve nearly

423　horizontally on the Van Krevelen diagram space, suggesting that hydroxylation is a

424　dominant reaction pathway during the aging process. This conclusion is consistent with

425　nano-DESI MS results, which demonstrate the presence of a wide range of abundant

426　hydroxylated molecules in phenolic aqSOA.

427　　　　　Overall, our results demonstrate that photochemical aging significantly transforms

428　the chemical composition and volatility distribution of phenolic aqSOA. Based on the

429　bulk and molecular results, phenolic aqSOA evolves dynamically during photochemical

430　aging, with different reaction pathways (oligomerization, fragmentation, and

431　functionalization) leading to different generations of products that span an enormous

432　range in volatilities and a large range in oxidation state and composition. Yee et al. (*2013*)

433　investigated the photooxidation of phenols under low-NO_x condition, and hydrogen

434　peroxide was used as the •OH precursor. The major reaction pathways include

435　demethoxylation and open-ring process, and oligomer formation is not observed in •OH-

436　initiated oxidation of phenols in the gas phase (*Yee et al., 2013*). The detection of a

437   number of compound with $C^* < 3.2 \times 10^{-4}$ μg m^{-3} suggests that aqueous reactions of

438   phenolic compounds are likely an important source of ELVOC in the atmosphere,

439   especially in regions strongly influenced by biomass burning emissions. While some of

440   these smaller, highly oxygenated species will be released to the gas phase, even at the

441   longest aging times the samples contain large, low volatility, derivatized oligomers that

442   are quite recalcitrant to fragmentation. The presence of presumably hygroscopic

443   hydroxylated carboxylic acids suggests these phenolic products might influence water

444   uptake in particles downwind of biomass burning. It is unclear whether the products we

445   identified here might influence the health effects of ambient particles.

446   **Appendix A. Comparisons between AMS and nano-DESI MS for average aqSOA**

447   **elemental composition analysis**

448   Figure A1 compares the average O/C, H/C, and OS$_C$ values, and the ΔO/C, ΔH/C,

449   and ΔOS$_C$ values between different reactions stages, of the 18 aqSOA samples measured

450   by the AMS versus those by the nano-DESI MS. The average O/C and H/C determined

451   by nano-DESI MS are systematically lower than those of bulk aqSOA measured by AMS,

452   which may be due to the assumption of equal ionization efficiency for all molecules

453   (*Bateman et al., 2009*) and the fact that molecules smaller than 100 Da, most of which

454   are highly oxidized, were outside of the operational mass range of nano-DESI MS. The

455   differences could also be exacerbated by the large differences between the AMS and the

456   nano-DESI MS methodology, in terms of sample analysis, data processing, and the

457   assumptions used for the average O/C calculations. Despite these differences in O/C and

458   H/C, OS$_C$ for phenolic aqSOA determined by nano-DESI MS and AMS agree well ($r^2 =$

459   0.71; slope = 1.01). In addition, ΔO/C and ΔOS$_C$ based on nano-DESI MS measurements

460 also appear to be systematically lower than those measured by AMS, but the two sets are

461 very well correlated (r^2 = 0.84 – 0.89; Fig. A1d-f). The correlations between the two

462 instruments are generally worse for H/C comparatively. These results suggest that

463 differences in O/C and OS_C of phenolic aqSOA formed at different reaction times

464 determined by nano-DESI MS are systematically lower by certain factors than those

465 measured by AMS for all reactions.

466 **Acknowledgement**

475

476 **References**

477 Aiken, A. C., Decarlo, P. F., Kroll, J. H., Worsnop, D. R., Huffman, J. A., Docherty, K.
478 S., Ulbrich, I. M., Mohr, C., Kimmel, J. R., Sueper, D., Sun, Y., Zhang, Q., Trimborn, A.,
479 Northway, M., Ziemann, P. J., Canagaratna, M. R., Onasch, T. B., Alfarra, M. R., Prevot, A. S. H.,
480 Dommen, J., Duplissy, J., Metzger, A., Baltensperger, U., and Jimenez, J. L.: O/c and om/oc
481 ratios of primary, secondary, and ambient organic aerosols with high-resolution time-of-flight
482 aerosol mass spectrometry, Environ. Sci. Technol., 42, 4478-4485, 10.1021/es703009q, 2008.

483 Altieri, K. E., Hastings, M. G., Peters, A. J., and Sigman, D. M.: Molecular
484 characterization of water soluble organic nitrogen in marine rainwater by ultra-high resolution
485 electrospray ionization mass spectrometry, Atmos Chem Phys, 12, 3557-3571, 10.5194/acp-12-
486 3557-2012, 2012.

487 Anastasio, C., Faust, B. C., and Rao, C. J.: Aromatic carbonyl compounds as aqueous-
488 phase photochemical sources of hydrogen peroxide in acidic sulfate aerosols, fogs, and clouds .1.

21

489   Non-phenolic methoxybenzaldehydes and methoxyacetophenones with reductants (phenols),
490   Environ. Sci. Technol., 31, 218-232, 10.1021/es960359g, 1997.

491   Andreae, M. O., and Gelencsér, A.: Black carbon or brown carbon? The nature of light-
492   absorbing carbonaceous aerosols, Atmos. Chem. Phys., 6, 3131-3148, 10.5194/acp-6-3131-2006,
493   2006.

494   Bateman, A. P., Nizkorodov, S. A., Laskin, J., and Laskin, A.: Time-resolved molecular
495   characterization of limonene/ozone aerosol using high-resolution electrospray ionization mass
496   spectrometry, Phys. Chem. Chem. Phys., 11, 7931-7942, 10.1039/b905288g, 2009.

497   Bateman, A. P., Laskin, J., Laskin, A., and Nizkorodov, S. A.: Applications of high-
498   resolution electrospray ionization mass spectrometry to measurements of average oxygen to
499   carbon ratios in secondary organic aerosols, Environ. Sci. Technol., 46, 8315-8324,
500   10.1021/es3017254, 2012.

501   Blando, J. D., and Turpin, B. J.: Secondary organic aerosol formation in cloud and fog
502   droplets: A literature evaluation of plausibility, Atmos. Environ., 34, 1623-1632, 10.1016/S1352-
503   2310(99)00392-1, 2000.

504   Chang, J. L., and Thompson, J. E.: Characterization of colored products formed during
505   irradiation of aqueous solutions containing h2o2 and phenolic compounds, Atmos. Environ., 44,
506   541-551, 10.1016/j.atmosenv.2009.10.042, 2010.

507   Collett, J. L., Hoag, K. J., Sherman, D. E., Bator, A., and Richards, L. W.: Spatial and
508   temporal variations in san joaquin valley fog chemistry, Atmospheric Environment, 33, 129-140,
509   1999.

510   Donahue, N. M., Kroll, J. H., Pandis, S. N., and Robinson, A. L.: A two-dimensional
511   volatility basis set – part 2: Diagnostics of organic-aerosol evolution, Atmos. Chem. Phys., 12,
512   615-634, 10.5194/acp-12-615-2012, 2012.

513   Ervens, B., Turpin, B. J., and Weber, R. J.: Secondary organic aerosol formation in cloud
514   droplets and aqueous particles (aqsoa): A review of laboratory, field and model studies, Atmos.
515   Chem. Phys., 11, 11069-11102, 10.5194/acp-11-11069-2011, 2011.

516   Ervens, B.: Modeling the processing of aerosol and trace gases in clouds and fogs, Chem.
517   Rev., 10.1021/cr5005887, 2015.

518   Feigenbrugel, V., Le Calvé, S., Mirabel, P., and Louis, F.: Henry's law constant
519   measurements for phenol, o-, m-, and p-cresol as a function of temperature, Atmospheric
520   Environment, 38, 5577-5588, http://dx.doi.org/10.1016/j.atmosenv.2004.06.025, 2004.

521   Ge, X. L., Zhang, Q., Sun, Y. L., Ruehl, C. R., and Setyan, A.: Effect of aqueous-phase
522   processing on aerosol chemistry and size distributions in fresno, california, during wintertime,
523   Environ. Chem., 9, 221-235, 10.1071/en11168, 2012.

524   George, K. M., Ruthenburg, T. C., Smith, J., Yu, L., Zhang, Q., Anastasio, C., and
525   Dillner, A. M.: Ft-ir quantification of the carbonyl functional group in aqueous-phase secondary
526   organic aerosol from phenols, Atmospheric Environment, 100, 230-237,
527   10.1016/j.atmosenv.2014.11.011, 2015.

528   Graber, E. R., and Rudich, Y.: Atmospheric hulis: How humic-like are they? A
529   comprehensive and critical review, Atmos. Chem. Phys., 6, 729-753, 10.5194/acp-6-729-2006,
530   2006.

531   Hallquist, M., Wenger, J. C., Baltensperger, U., Rudich, Y., Simpson, D., Claeys, M.,
532   Dommen, J., Donahue, N. M., George, C., Goldstein, A. H., Hamilton, J. F., Herrmann, H.,
533   Hoffmann, T., Iinuma, Y., Jang, M., Jenkin, M. E., Jimenez, J. L., Kiendler-Scharr, A., Maenhaut,
534   W., McFiggans, G., Mentel, T. F., Monod, A., Prevot, A. S. H., Seinfeld, J. H., Surratt, J. D.,
535   Szmigielski, R., and Wildt, J.: The formation, properties and impact of secondary organic aerosol:
536   Current and emerging issues, Atmos. Chem. Phys., 9, 5155-5236, 10.5194/acp-9-5155-2009,
537   2009.

538   Hawthorne, S. B., Krieger, M. S., Miller, D. J., and Mathiason, M. B.: Collection and
539   quantitation of methoxylated phenol tracers for atmospheric-pollution from residential wood
540   stoves, Environ. Sci. Technol., 23, 470-475, 10.1021/es00181a013, 1989.

541   Hennigan, C. J., Westervelt, D. M., Riipinen, I., Engelhart, G. J., Lee, T., Collett, J. L.,
542   Pandis, S. N., Adams, P. J., and Robinson, A. L.: New particle formation and growth in biomass
543   burning plumes: An important source of cloud condensation nuclei, Geophysical Research Letters,
544   39, 10.1029/2012gl050930, 2012.

545   Herrmann, H.: Kinetics of aqueous phase reactions relevant for atmospheric chemistry,
546   Chem. Rev., 103, 4691-4716, 10.1021/cr020658q, 2003.

547   Jimenez, J. L., Canagaratna, M. R., Donahue, N. M., Prevot, A. S. H., Zhang, Q., Kroll, J.
548   H., DeCarlo, P. F., Allan, J. D., Coe, H., Ng, N. L., Aiken, A. C., Docherty, K. S., Ulbrich, I. M.,
549   Grieshop, A. P., Robinson, A. L., Duplissy, J., Smith, J. D., Wilson, K. R., Lanz, V. A., Hueglin,
550   C., Sun, Y. L., Tian, J., Laaksonen, A., Raatikainen, T., Rautiainen, J., Vaattovaara, P., Ehn, M.,
551   Kulmala, M., Tomlinson, J. M., Collins, D. R., Cubison, M. J., Dunlea, E. J., Huffman, J. A.,
552   Onasch, T. B., Alfarra, M. R., Williams, P. I., Bower, K., Kondo, Y., Schneider, J., Drewnick, F.,
553   Borrmann, S., Weimer, S., Demerjian, K., Salcedo, D., Cottrell, L., Griffin, R., Takami, A.,
554   Miyoshi, T., Hatakeyama, S., Shimono, A., Sun, J. Y., Zhang, Y. M., Dzepina, K., Kimmel, J. R.,
555   Sueper, D., Jayne, J. T., Herndon, S. C., Trimborn, A. M., Williams, L. R., Wood, E. C.,
556   Middlebrook, A. M., Kolb, C. E., Baltensperger, U., and Worsnop, D. R.: Evolution of organic
557   aerosols in the atmosphere, Science, 326, 1525-1529, 10.1126/science.1180353, 2009.

558   Kroll, J. H., and Seinfeld, J. H.: Chemistry of secondary organic aerosol: Formation and
559   evolution of low-volatility organics in the atmosphere, Atmospheric Environment, 42, 3593-3624,
560   10.1016/j.atmosenv.2008.01.003, 2008.

561   Kroll, J. H., Smith, J. D., Che, D. L., Kessler, S. H., Worsnop, D. R., and Wilson, K. R.:
562   Measurement of fragmentation and functionalization pathways in the heterogeneous oxidation of
563   oxidized organic aerosol, Phys. Chem. Chem. Phys., 11, 8005-8014, 10.1039/B905289E, 2009.

564   Kroll, J. H., Donahue, N. M., Jimenez, J. L., Kessler, S. H., Canagaratna, M. R., Wilson,
565   K. R., Altieri, K. E., Mazzoleni, L. R., Wozniak, A. S., Bluhm, H., Mysak, E. R., Smith, J. D.,
566   Kolb, C. E., and Worsnop, D. R.: Carbon oxidation state as a metric for describing the chemistry
567   of atmospheric organic aerosol, Nat. Chem., 3, 133-139, 10.1038/nchem.948, 2011.

568   Laskin, A., Laskin, J., and Nizkorodov, S. A.: Chemistry of atmospheric brown carbon,
569   Chem. Rev., 10.1021/cr5006167, 2015.

23

Lee, A. K. Y., Hayden, K. L., Herckes, P., Leaitch, W. R., Liggio, J., Macdonald, A. M., and Abbatt, J. P. D.: Characterization of aerosol and cloud water at a mountain site during wacs 2010: Secondary organic aerosol formation through oxidative cloud processing, Atmos. Chem. Phys., 12, 7103-7116, 10.5194/acp-12-7103-2012, 2012.

Lee, H. J., Aiona, P. K., Laskin, A., Laskin, J., and Nizkorodov, S. A.: Effect of solar radiation on the optical properties and molecular composition of laboratory proxies of atmospheric brown carbon, Environmental Science & Technology, 48, 10217-10226, 10.1021/es502515r, 2014.

Lim, Y. B., Tan, Y., Perri, M. J., Seitzinger, S. P., and Turpin, B. J.: Aqueous chemistry and its role in secondary organic aerosol (soa) formation, Atmos Chem Phys, 10, 10521-10539, 10.5194/acp-10-10521-2010, 2010.

Morgan, W. T., Allan, J. D., Bower, K. N., Highwood, E. J., Liu, D., McMeeking, G. R., Northway, M. J., Williams, P. I., Krejci, R., and Coe, H.: Airborne measurements of the spatial distribution of aerosol chemical composition across europe and evolution of the organic fraction, Atmos. Chem. Phys., 10, 4065-4083, 10.5194/acp-10-4065-2010, 2010.

Nannoolal, Y., Rarey, J., Ramjugernath, D., and Cordes, W.: Estimation of pure component properties: Part 1. Estimation of the normal boiling point of non-electrolyte organic compounds via group contributions and group interactions, Fluid Phase Equilibria, 226, 45-63, 10.1016/j.fluid.2004.09.001, 2004.

Nannoolal, Y., Rarey, J., and Ramjugernath, D.: Estimation of pure component properties: Part 3. Estimation of the vapor pressure of non-electrolyte organic compounds via group contributions and group interactions, Fluid Phase Equilibria, 269, 117-133, 10.1016/j.fluid.2008.04.020, 2008.

Ng, N. L., Canagaratna, M. R., Zhang, Q., Jimenez, J. L., Tian, J., Ulbrich, I. M., Kroll, J. H., Docherty, K. S., Chhabra, P. S., Bahreini, R., Murphy, S. M., Seinfeld, J. H., Hildebrandt, L., Donahue, N. M., DeCarlo, P. F., Lanz, V. A., Prévôt, A. S. H., Dinar, E., Rudich, Y., and Worsnop, D. R.: Organic aerosol components observed in northern hemispheric datasets from aerosol mass spectrometry, Atmos. Chem. Phys., 10, 4625-4641, 10.5194/acp-10-4625-2010, 2010.

Pankow, J. F., and Barsanti, K. C.: The carbon number-polarity grid: A means to manage the complexity of the mix of organic compounds when modeling atmospheric organic particulate matter, Atmospheric Environment, 43, 2829-2835, 10.1016/j.atmosenv.2008.12.050, 2009.

Renard, P., Siekmann, F., Salque, G., Demelas, C., Coulomb, B., Vassalo, L., Ravier, S., Temime-Roussel, B., Voisin, D., and Monod, A.: Aqueous-phase oligomerization of methyl vinyl ketone through photooxidation – part 1: Aging processes of oligomers, Atmos. Chem. Phys., 15, 21-35, 10.5194/acp-15-21-2015, 2015.

Roach, P. J., Laskin, J., and Laskin, A.: Molecular characterization of organic aerosols using nanospray-desorption/electrospray ionization-mass spectrometry, Anal. Chem., 82, 7979-7986, 10.1021/ac101449p, 2010a.

609   Roach, P. J., Laskin, J., and Laskin, A.: Nanospray desorption electrospray ionization: An
610 ambient method for liquid-extraction surface sampling in mass spectrometry, Analyst, 135, 2233-
611 2236, 10.1039/c0an00312c, 2010b.

612   Romonosky, D. E., Laskin, A., Laskin, J., and Nizkorodov, S. A.: High-resolution mass
613 spectrometry and molecular characterization of aqueous photochemistry products of common
614 types of secondary organic aerosols, The Journal of Physical Chemistry A, 119, 2594-2606,
615 10.1021/jp509476r, 2015.

616   Sagebiel, J. C., and Seiber, J. N.: Studies on the occurrence and distribution of wood
617 smoke marker compounds in foggy atmospheres, Environ. Toxicol. Chem., 12, 813-822,
618 10.1002/etc.5620120504, 1993.

619   Schauer, J. J., Kleeman, M. J., Cass, G. R., and Simoneit, B. R. T.: Measurement of
620 emissions from air pollution sources. 3. C-1-c-29 organic compounds from fireplace combustion
621 of wood, Environ. Sci. Technol., 35, 1716-1728, 10.1021/es001331e, 2001.

622   Smith, J. D., Sio, V., Yu, L., Zhang, Q., and Anastasio, C.: Secondary organic aerosol
623 production from aqueous reactions of atmospheric phenols with an organic triplet excited state,
624 Environ. Sci. Technol., 48, 1049-1057, 10.1021/es4045715, 2014.

625   Smith, J. D., Kinney, H., and Anastasio, C.: Aqueous benzene-diols react with an organic
626 triplet excited state and hydroxyl radical to form secondary organic aerosol, Phys. Chem. Chem.
627 Phys., 10.1039/C4CP06095D, 2015.

628   Sun, Y., Zhang, Q., Macdonald, A. M., Hayden, K., Li, S. M., Liggio, J., Liu, P. S. K.,
629 Anlauf, K. G., Leaitch, W. R., Steffen, A., Cubison, M., Worsnop, D. R., van Donkelaar, A., and
630 Martin, R. V.: Size-resolved aerosol chemistry on whistler mountain, canada with a high-
631 resolution aerosol mass spectrometer during intex-b, Atmos. Chem. Phys., 9, 3095-3111,
632 10.5194/acp-9-3095-2009, 2009.

633   Sun, Y. L., Zhang, Q., Anastasio, C., and Sun, J.: Insights into secondary organic aerosol
634 formed via aqueous-phase reactions of phenolic compounds based on high resolution mass
635 spectrometry, Atmos. Chem. Phys., 10, 4809-4822, 10.5194/acp-10-4809-2010, 2010.

636   Yasmeen, F., Vermeylen, R., Szmigielski, R., Iinuma, Y., Böge, O., Herrmann, H.,
637 Maenhaut, W., and Claeys, M.: Terpenylic acid and related compounds: Precursors for dimers in
638 secondary organic aerosol from the ozonolysis of α and β-pinene, Atmos. Chem.
639 Phys. Discuss., 10, 10865-10888, 10.5194/acpd-10-10865-2010, 2010.

640   Yee, L. D., Kautzman, K. E., Loza, C. L., Schilling, K. A., Coggon, M. M., Chhabra, P.
641 S., Chan, M. N., Chan, A. W. H., Hersey, S. P., Crounse, J. D., Wennberg, P. O., Flagan, R. C.,
642 and Seinfeld, J. H.: Secondary organic aerosol formation from biomass burning intermediates:
643 Phenol and methoxyphenols, Atmos. Chem. Phys., 13, 8019-8043, 10.5194/acp-13-8019-2013,
644 2013.

645   Yu, L., Smith, J., Laskin, A., Anastasio, C., Laskin, J., and Zhang, Q.: Chemical
646 characterization of soa formed from aqueous-phase reactions of phenols with the triplet excited
647 state of carbonyl and hydroxyl radical, Atmos. Chem. Phys., 14, 13801-13816, 10.5194/acp-14-
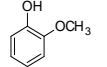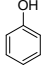648 13801-2014, 2014.

25
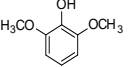
649   Zhang, Q., and Anastasio, C.: Conversion of fogwater and aerosol organic nitrogen to
650 ammonium, nitrate, and nox during exposure to simulated sunlight and ozone, Environmental
651 Science & Technology, 37, 3522-3530, 10.1021/es034114x, 2003.

652   Zhang, Q., Jimenez, J. L., Canagaratna, M. R., Allan, J. D., Coe, H., Ulbrich, I., Alfarra,
653 M. R., Takami, A., Middlebrook, A. M., Sun, Y. L., Dzepina, K., Dunlea, E., Docherty, K.,
654 DeCarlo, P. F., Salcedo, D., Onasch, T., Jayne, J. T., Miyoshi, T., Shimono, A., Hatakeyama, S.,
655 Takegawa, N., Kondo, Y., Schneider, J., Drewnick, F., Borrmann, S., Weimer, S., Demerjian, K.,
656 Williams, P., Bower, K., Bahreini, R., Cottrell, L., Griffin, R. J., Rautiainen, J., Sun, J. Y., Zhang,
657 Y. M., and Worsnop, D. R.: Ubiquity and dominance of oxygenated species in organic aerosols in
658 anthropogenically-influenced northern hemisphere midlatitudes, Geophys. Res. Lett., 34, L13801,
659 10.1029/2007GL029979, 2007.
660
661

26

662 **Tables and Figures**

663 **Table 1** Summary of the chemical characteristics of phenolic aqSOA formed during different stages of photoreaction

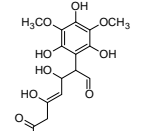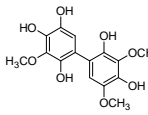| Precursor information			Syringol (SYR) H_3CO—OH—OCH_3			Guaiacol (GUA) OH—OCH_3			Phenol (PhOH) OH		
		ID and chemical structure									
		Chemical formula (MW)	$C_8H_{10}O_3$ (154)			$C_7H_8O_2$ (124)			C_6H_6O (94)		
		Henry's law constant (M atm^{-1})	2.5×10^4			5.0×10^3			1.5×10^4		
		O/C, H/C, OS$_C$	0.38, 1.25, -0.50			0.29, 1.14, -0.57			0.17, 1.00, -0.67		
Reaction interval (hrs)			**P1**	**P2**	**P3**	**P1**	**P2**	**P3**	**P1**	**P2**	**P3**
		•OH	0-2	2-4	4-6	0-2	2-4	4-6	0-6	6-12	23-24
		^{3}C*	0-2	2-4	4-6	0-2	2-4	4-6	0-5	5-9	19-20
aqSOA measurements	AMS	O/C •OH	0.87	0.92	0.96	0.80	0.88	0.95	0.77	0.85	1.03
		O/C ^{3}C*	0.81	0.94	0.97	0.66	0.73	0.76	0.67	0.79	1.00
		H/C •OH	1.69	1.66	1.67	1.70	1.69	1.69	1.56	1.55	1.54
		H/C ^{3}C*	1.48	1.52	1.53	1.44	1.39	1.38	1.45	1.43	1.55
		OS$_C$ •OH	0.05	0.18	0.25	-0.1	0.07	0.21	-0.02	0.15	0.52
		OS$_C$ ^{3}C*	0.14	0.36	0.41	-0.12	0.07	0.14	-0.11	0.15	0.45
	(-) nano-DESI MS	# of molecules •OH	641	877	668	238	352	373	56	389	483
		# of molecules ^{3}C*	571	697	627	331	656	696	156	617	405
		Avg. formula •OH	$C_{14.0}H_{14.4}O_{7.4}$	$C_{13.1}H_{13.2}O_{7.9}$	$C_{11.7}H_{12.0}O_{7.6}$	$C_{15.2}H_{13.9}O_{5.7}$	$C_{14.4}H_{13.1}O_{5.8}$	$C_{13.6}H_{12.3}O_{6.1}$	$C_{12.6}H_{9.9}O_{4.3}$	$C_{12.3}H_{10.1}O_{5.3}$	$C_{9.9}H_{8.9}O_{5.6}$
		Avg. formula ^{3}C*	$C_{14.1}H_{14.2}O_{8.2}$	$C_{11.4}H_{11.8}O_{7.8}$	$C_{10.8}H_{11.4}O_{7.5}$	$C_{17.1}H_{15.9}O_{6.0}$	$C_{17.0}H_{15.4}O_{6.6}$	$C_{16.3}H_{14.7}O_{6.7}$	$C_{16.1}H_{12.2}O_{4.0}$	$C_{15.5}H_{11.7}O_{5.1}$	$C_{10.2}H_{8.8}O_{5.1}$
		Avg. MW •OH	300.9	296.9	274.1	287.6	278.8	273.2	230.0	242.6	217.3
		Avg. MW ^{3}C*	314.7	273.5	261.1	317.2	325.1	317.6	269.5	279.4	212.8
		O/C •OH	0.53	0.60	0.64	0.37	0.41	0.45	0.34	0.43	0.57
		O/C ^{3}C*	0.59	0.68	0.69	0.35	0.38	0.41	0.25	0.33	0.49
		H/C •OH	1.03	1.01	1.02	0.92	0.91	0.91	0.79	0.82	0.9
		H/C ^{3}C*	1.02	1.03	1.05	0.93	0.90	0.90	0.76	0.76	0.86
		OS$_C$ •OH	0.03	0.19	0.26	-0.18	-0.09	-0.01	-0.11	0.04	0.24
		OS$_C$ ^{3}C*	0.16	0.33	0.33	-0.23	-0.14	-0.08	-0.26	-0.10	0.12
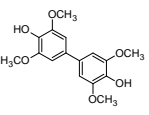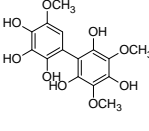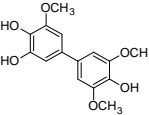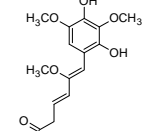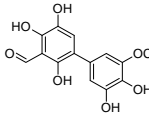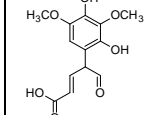
664

665 **Table 2** Summary of the kinetics of the destructions of phenolic precursors and formation of
666 aqSOA during simulated sunlight illumination. The error range calculation is based on the 95%
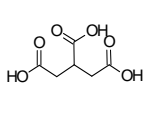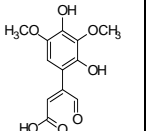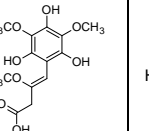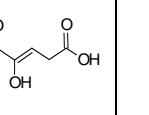667 confidential interval.
668
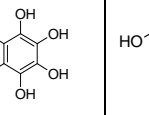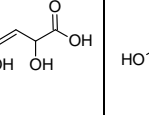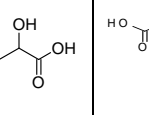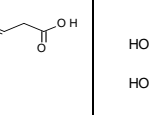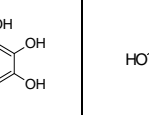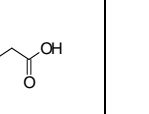
	SYR		GUA		PhOH	
	•OH	^{3}C*	•OH	^{3}C*	•OH	^{3}C*
Rate constant of phenol decay k_d (hr^{-1})	0.80±0.2	2.0±0.0	0.40±0.08	0.97±0.17	0.05±0.02	0.090±0.019
Initial decay rate of phenol R_d (mg L^{-1} hr^{-1})	12±3.0	30±0.6	4.1±0.81	10±1.8	0.50±0.19	0.91±0.19
Rate constant of aqSOA formation k_f (hr^{-1})	0.82±0.03	1.1±0.03	0.08±0.01	0.51±0.01	0.015*	0.018*
Initial formation rate of aqSOA R_f (mg L^{-1} hr^{-1})	14±0.53	16±.44	1.6±0.20	4.1±0.08	0.65*	0.82*

669
670 *The fitted values have very large uncertainties.

Table 3 Most abundant compounds identified in SYR aqSOA formed during different stages of the $^3C^*$-mediated reactions.

No		1	2	3	4	5	6	7	8
Molecular formula[a]		$C_{16}H_{18}O_6$ (306.1103)	$C_{15}H_{16}O_9$ (340.0794)	$C_{15}H_{16}O_6$ (292.0946)	$C_{15}H_{18}O_7$ (310.1052)	$C_{14}H_{12}O_7$ (292.0583)	$C_{13}H_{14}O_7$ (282.0739)	$C_{15}H_{18}O_{10}$ (358.0900)	$C_{15}H_{16}O_8$ (324.0845)
Proposed structure									
$C^{*\,b}$ ($\mu g\ m^{-3}$)		3.1E-03	3.9E-12	3.4E-04	1.7E-05	6.6E-09	1.8E-05	1.5E-13	2.8E-09
Relative abundance (ranking)[c]	P1: 0-2 hrs	100 (1)	80 (2)	70 (3)	67 (4)	60 (5)	48 (6)	44 (7)	44 (8)
	P2: 2-4 hrs	0.0 (NA)	100 (1)	0.7 (518)	15 (62)	8.9 (128)	21 (33)	42 (7)	11 (93)
	P3: 4-6 hrs	0.0 (NA)	100 (1)	0.3 (575)	4.0 (230)	5.1 (203)	19 (42)	41 (7)	8.1 (141)

| 9	10	11	12	13	14	15	16	17	18
$C_6H_8O_6$ (176.0321)	$C_{12}H_{12}O_7$ (268.0583)	$C_{13}H_{16}O_8$ (300.0845)	$C_5H_6O_5$ (146.0215)	$C_6H_6O_6$ (174.0164)	$C_5H_6O_6$ (162.0164)	$C_4H_6O_5$ (134.0215)	$C_5H_6O_4$ (130.0266)	$C_6H_6O_5$ (158.0215)	$C_4H_6O_4$ (118.0266)
2.2E-02	1.3E-07	3.4E-07	2.7E+01	5.2E-05	5.0E-02	4.2E+00	5.0E+02	2.2E-02	2.9E+00
39 (9)	37 (10)	33 (12)	21 (25)	17 (37)	17 (39)	14 (48)	11 (70)	10 (76)	0.0 (NA)
81 (2)	32 (10)	36 (9)	31 (11)	46 (6)	52 (3)	50 (4)	40 (8)	30 (12)	48 (5)
83 (2)	29 (13)	35 (10)	36 (9)	63 (4)	46 (5)	78 (3)	45 (6)	39 (8)	0.0 (NA)

674 [a] Molecular formulas and proposed structures of 18 compounds identified according to (-) nano-DESI spectra. They represent the top
675 10 most abundant aqSOA compounds observed at each reaction stage. The exact molecular weight of each compound is shown in
676 parentheses.
677 [b] Estimated saturation concentrations (C^*, μg m^{-3}) of the compounds at 25 ∘C, 1 atm, determined using the Nannoolal vapor pressure
678 and extrapolation method.
679 [c] Relative abundances (%) of the compounds and, in parentheses, their abundance ranks counted in the sorted relative abundance list of
680 all the compounds identified in the nano-DESI mass spectrum of the specified time period.

30

681
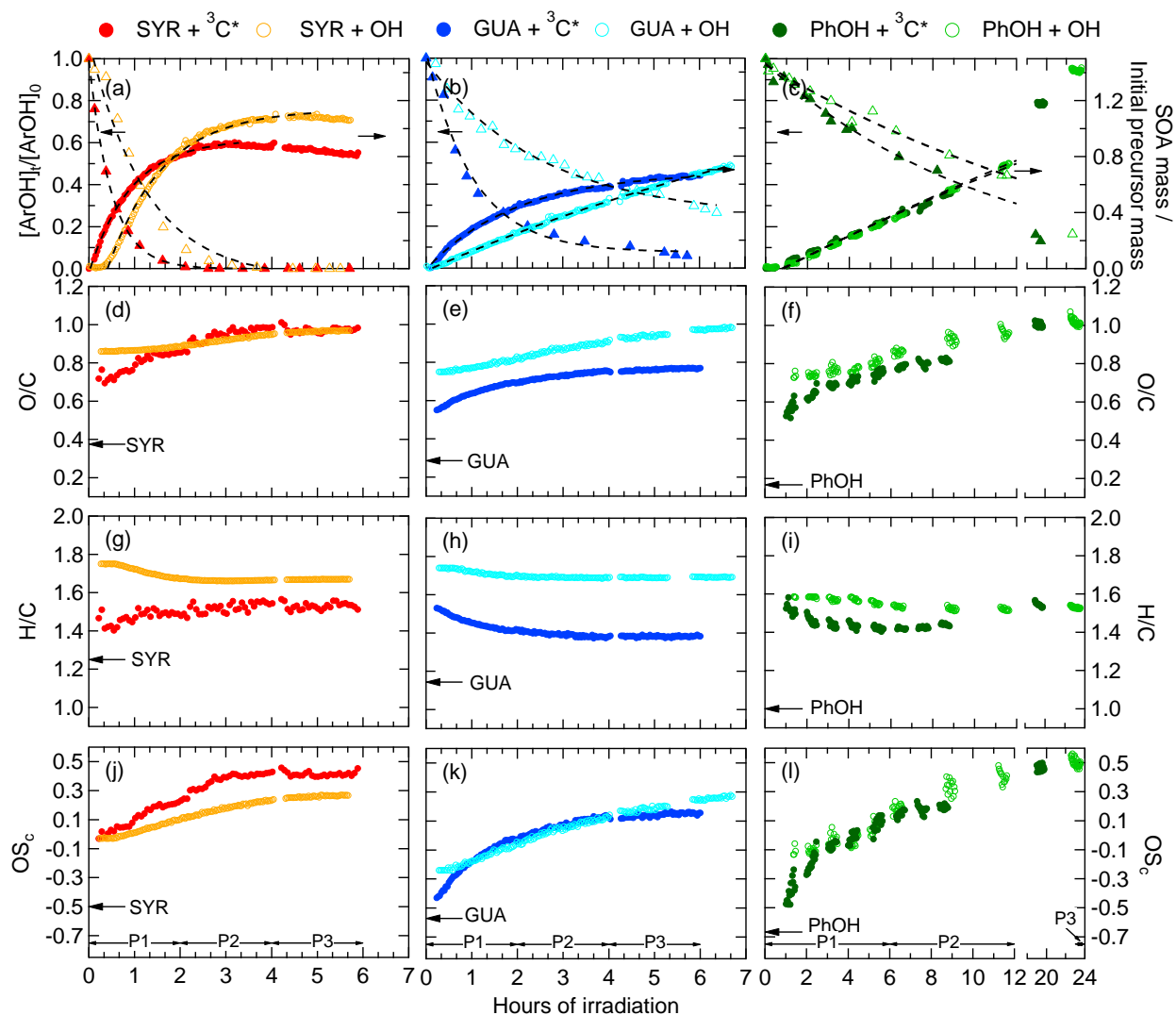
Figure 1. Evolution of **(a-c)** concentration of phenol precursors (left axes) and aqSOA mass (right axes) normalized by the initial concentration of precursor, **(d-f)** O/C of aqSOA, **(g-i)** H/C of aqSOA, and **(j-l)** OS_C of aqSOA as a function of reaction time during individual experiments. The aqSOA mass and elemental ratios are determined from AMS data and precursor concentrations are measured by HPLC. In **(a-c)**, phenol precursors are represented by solid and open triangles and aqSOA by solid and open circles. The two different oxidants are represented by the symbols shown in the legend on the top of the figure. The lines in **(a-c)** represent the regression fits to each set of experimental data and the fit parameters are summarized in Table 2. The O/C, H/C, and OS_C values of individual phenolic precursors are indicated by the arrows in **(d-l)**. The 3 reaction periods (P1 – P3) for which filter samples were collected for nano-DESI MS analyses are marked in **(j-l)**.

693

31
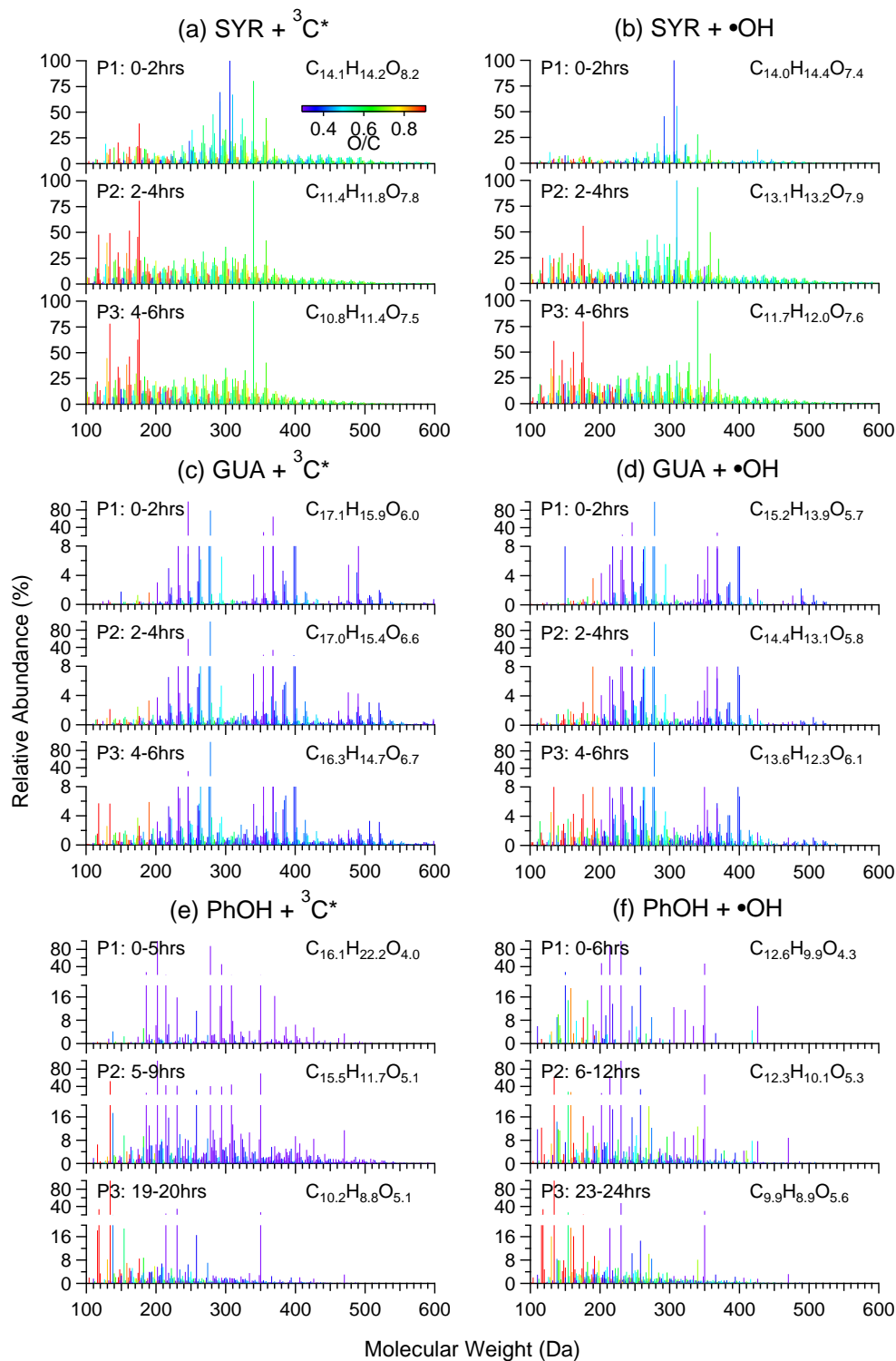
Figure 2. Negative ion mode nano-DESI mass spectra of phenolic aqSOA formed during different stages of photoreaction. Signals are colored by the O/C ratios of the molecules. The signal-weighted average molecular formula of each aqSOA is shown in the legends.
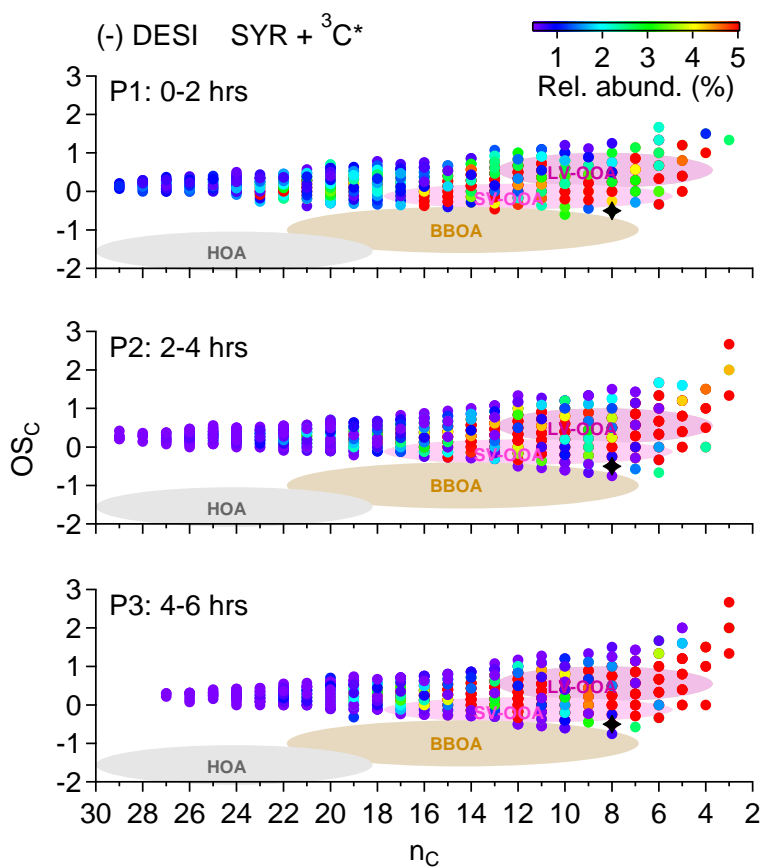
Figure 3. OS_C and n_C of SYR aqSOA formed during different stages of $^3C^*$-mediated reactions determined based on (-) nano-DESI MS spectra. Signals are colored by the relative abundance of the molecules. The black star at $n_C = 8$ represents SYR. The shaded ovals indicate locations of different ambient organic aerosol classes reported in Kroll et al. (*2011*).
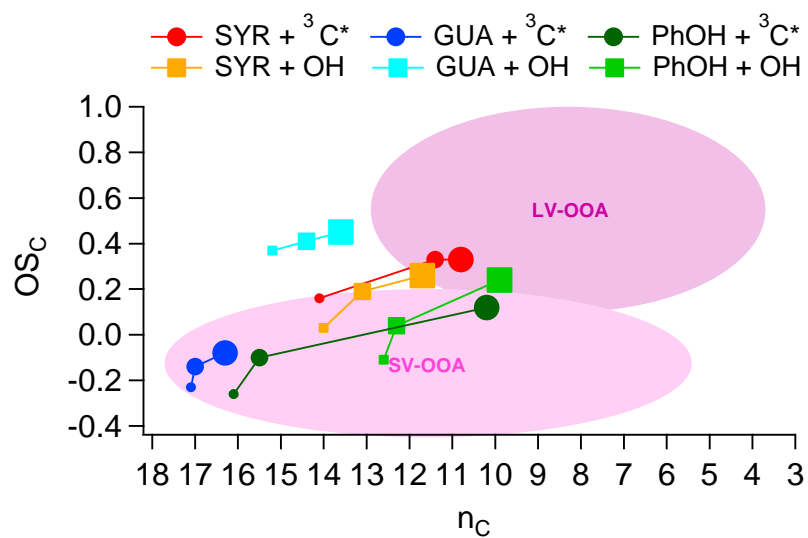
Figure 4. Average OS_C and n_C of phenolic aqSOA formed during different stages of $^3C^*$- and •OH-mediated reactions determined based on (-) nano-DESI MS data. The different phenolic and oxidant conditions are represented by the symbols shown in the legend. The symbol sizes increase with irradiation time. The shaded ovals indicate regions of LV-OOA and SV-OOA reported in Kroll et al. (*2011*).
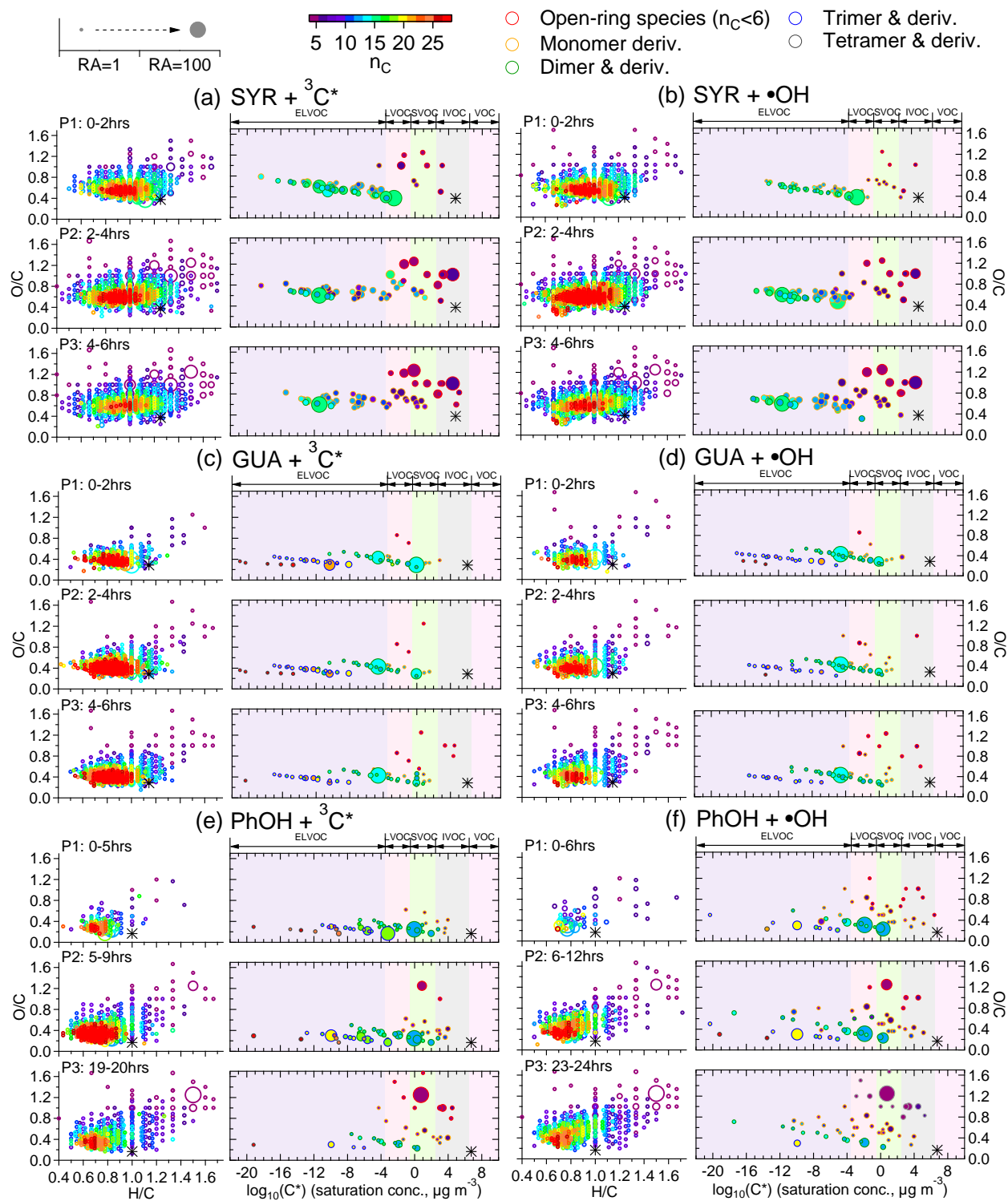
**Figure 5**. O/C and H/C of SYR, GUA and PhOH aqSOA molecules formed during three different stages of the $^3C^*$- and •OH-mediated reactions. To the right of each O/C vs. H/C plot is a plot that shows the O/C and volatility ($\log_{10} C^*$ in µg m^{-3}) for the 50 most abundant aqSOA molecules. On the O/C vs. C^* plots, the volatility ranges are indicated by colored bands: 1)

35

716　ELVOC ($C^* < 3.2 \times 10^{-4}$ µg m^{-3}), 2) LVOC (3.2×10^{-4} µg m^{-3} < C^* < 0.32 µg m^{-3}), 3) SVOC
717　(0.32 µg m^{-3} < C^* < 320 µg m^{-3}), 4) IVOC (320 µg m^{-3} < C^* < 3.2×10^6 µg m^{-3}), and 5) VOC (C^* >
718　3.2×10^6 µg m^{-3}). On the O/C vs. C^* plots, the degree of oligomerization for each species is
719　represented by the stroke color. On both O/C vs. H/C and O/C vs. C^* plots, sizes of points are
720　scaled by the relative abundance (RA) and colored by the number of carbon atoms (n_C). The
721　black stars represent phenolic precursors.
722

723
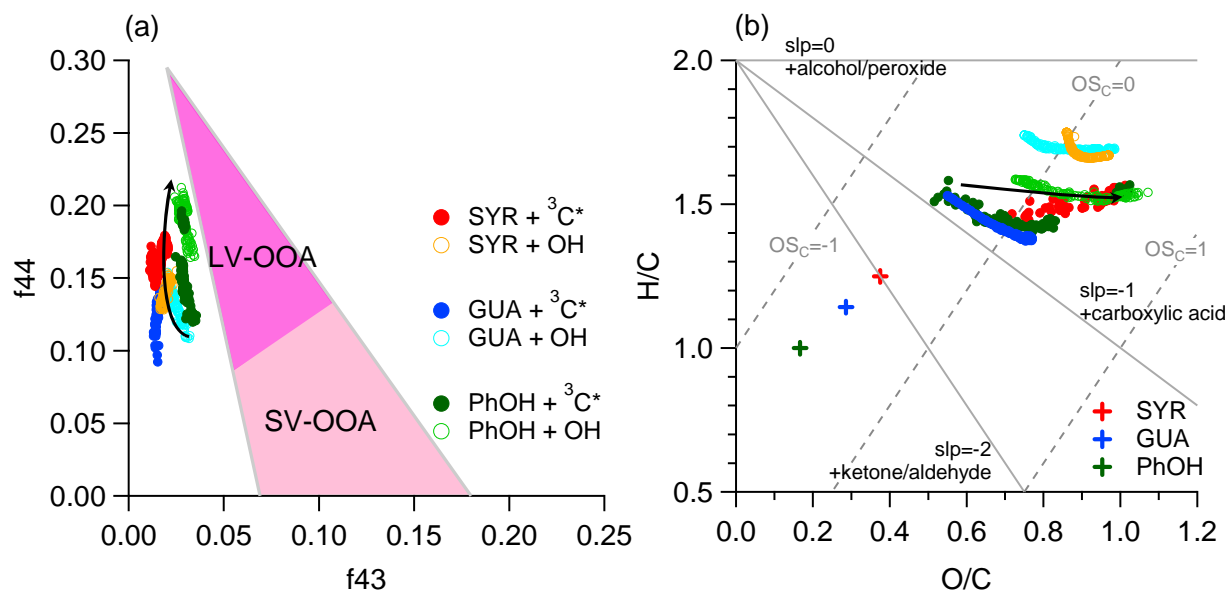
724

725　**Figure 6.** Evolution profiles of phenolic aqSOA in **(a)** the f_{44} vs. f_{43} space and **(b)** the H/C vs.
726　O/C space based on AMS measurements. The shaded triangle in (a) defines the region where
727　typical ambient SOA lie (*Ng et al., 2010*). Different experimental conditions are represented by
728　the symbols shown in the legend. Phenolic precursors are represented by the "+" symbols in (b).
729　Lines with slopes of 0, -1 and -2 indicate the addition of alcohol/peroxide, carboxylic acid, and
730　ketone/aldehyde functional group, respectively. Dashed lines indicate OS$_C$ of -1, 0 and 1,
731　respectively.
732

734
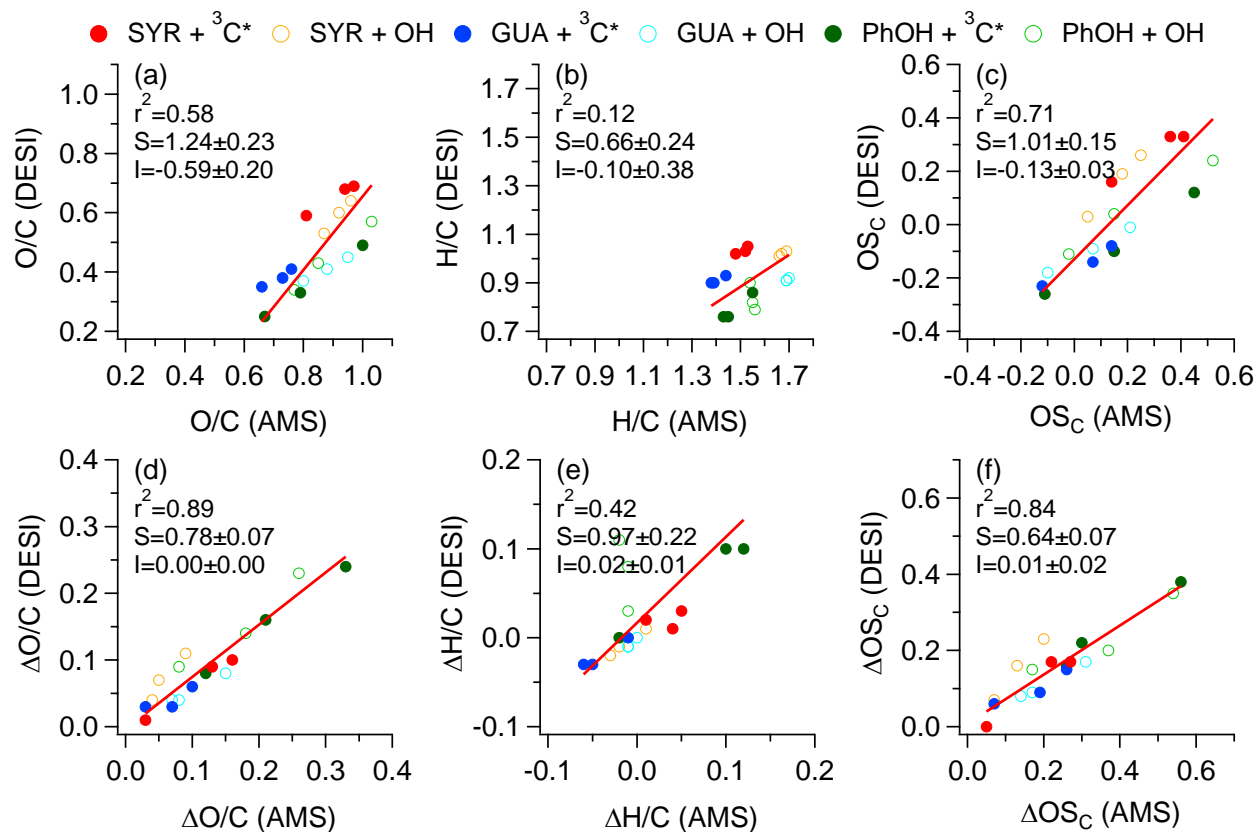
Figure A1. Scatter plots that compare nano-DESI MS and AMS measurements of the average **(a)** O/C, **(b)** H/C, **(c)** OS_C of aqSOA formed during 3 different stages of photoreaction and **(d)** ΔO/C, **(e)** ΔH/C, and **(f)** ΔOS_C between different stages. The Δ denotes the difference between different reaction stages (i.e., P2-P1, P3-P2, P3-P1). All linear regressions were performed using orthogonal distance regression (ODR) and the slopes (S), intercepts (I), and correlation coefficients (r^2) are shown in the legends. Different experimental conditions are represented by the symbols shown in the legend. The O/C, H/C and OS_C values shown here are also summarized in Table 1.